

## FULL PAPER

# Density functional theory/B3LYP study of nanometric 4-(2,4-dihydroxy-5-formylphen-1-ylazo)-*N*-(4-methylpyrimidin-2-yl) benzenesulfonamide complexes: Quantitative structure–activity relationship, docking, spectral and biological investigations

Fawaz A. Saad<sup>1</sup> | Marwa G. Elghalban<sup>1,2</sup> | Nashwa M. El-Metwaly<sup>1,2</sup> | Hoda El-Ghamry<sup>1,3</sup> | Abdalla M. Khedr<sup>1,3</sup>

<sup>1</sup>Department of Chemistry, Faculty of Applied Science, Umm Al-Qura University, Makkah, Saudi Arabia

<sup>2</sup>Chemistry Department, Faculty of Science, Mansoura University, Mansoura, Egypt

<sup>3</sup>Chemistry Department, Faculty of Science, Tanta University, Tanta, Egypt

**Correspondence**

Fawaz A. Saad, Department of Chemistry, Faculty of Applied Science, Umm Al-Qura University, Makkah, Saudi Arabia.

Email: fasaad@uqu.edu.sa

New metal ion complexes were isolated after coupling with 4-(2,4-dihydroxy-5-formylphen-1-ylazo)-*N*-(4-methylpyrimidin-2-yl)benzenesulfonamide (H<sub>2</sub>L) drug ligand. The structural and molecular formulae of drug derivative and its complexes were elucidated using spectral, analytical and theoretical tools. Vibrational spectral data proved that H<sub>2</sub>L behaves as a monobasic bidentate ligand through one nitrogen from azo group and ionized hydroxyl oxygen towards all metal ions. UV–visible and magnetic moment measurements indicated that Fe(III), Cr(III), Mn(II) and Ni(II) complexes have octahedral configuration whereas Cd(II), Zn(II) and Co(II) complexes are in tetrahedral form. The Cu(II) complex has square planar geometry as verified through electron spin resonance essential parameters. X-ray diffraction data indicated the amorphous nature of all compounds with no regular arrangement for the solid constituents during the precipitation process. Transmission electron microscopy images showed homogeneous metal ion distribution on the surface of the complexes with nanometric particles. Coats–Redfern equations were applied for calculating thermo-kinetic parameters for suitable thermal decomposition stages. Gaussian09 and quantitative structure–activity relationship modelling studies were used to verify the structural and biological features. Docking study using microorganism protein receptors was implemented to throw light on the biological behaviour of the proposed drug. The investigated ligand and metal complexes were screened for their *in vitro* antimicrobial activities against fungal and bacterial strains. The resulting data indicated that the investigated compounds are highly promising bactericides and fungicides. The antitumour activities of all compounds were evaluated towards human liver carcinoma (HEPG2) cell line.

**KEYWORDS**

antitumour and antimicrobial studies, azodye, docking, nanometre complexes, QSAR, spectral characterization

## 1 | INTRODUCTION

Diverse research studies have been published related to the synthesis and spectral properties of azodye compounds.<sup>[1–3]</sup> This reflects their significant applications in distinct fields such as in colouring fibres,<sup>[4]</sup> optical storage technology<sup>[5]</sup>

and photoelectronic implementations,<sup>[6]</sup> as well as their involvement in many analytical and biological applications.<sup>[7,8]</sup> Metal complexes of azodyes have also attracted increasing attention due to their interesting geometrical and electronic features. Their applications include printing systems, nonlinear optical elements, molecular memory storages

and others.<sup>[9,10]</sup> Also, sulfonamide derivatives resulting from the exchanges of diverse functional groups, while retaining the leading structural feature of sulfonamides, can present a range of promising pharmacological and medicinal activities.<sup>[11,12]</sup> Additionally, other basic moieties in sulfonamide compounds, such as aromatic amino groups, represent the main reason for the chemical multitude of such compounds because they can act as chelation centres. These can be considered as the reactive site for chemical modifications of sulfonamide ligands to afford a large number of complexes with great biological importance. Furthermore, sulfonamides and azodye derivatives of sulfonamides were found to have a variety of biological properties such as anti-tubercular, anticancer and antimalarial activities.<sup>[13]</sup> Many sulfonamide azodye derivatives are usually applied as powerful ligands for a vast range of transition metal ions.<sup>[14–16]</sup> The metal chelates find many applications in biological systems, dyeing processes and analytical detection of various metal ions.<sup>[17,18]</sup> Among sulfonamide derivatives, 4-amino-*N*-(4-methylpyrimidin-2-yl)benzenesulfonamide is well known as one of the most widely clinically applied chemical compounds.<sup>[19]</sup>

Based on the above considerations and in continuation of our research works,<sup>[20–22]</sup> the present paper reports the synthesis and characterization of a novel series of bioactive nano-sized and transition metal complexes with 4-(2,4-dihydroxy-5-formylphen-1-ylazo)-*N*-(4-methylpyrimidin-2-yl)benzenesulfonamide ( $H_2L$ ). The choice of azo compounds leads to a detailed spectral study as well as theoretical aspects. The nanometre scale of the complexes may serve excellently in the biological field which was considered the main goal in the study reported here. The investigated compounds were screened *in vitro* for their antitumour and antimicrobial activities. Computational studies were used to emphasize the structural and biological features to deepen the study.

## 2 | EXPERIMENTAL

All the reagents and solvents utilized in this work were of reagent-grade quality and applied as purchased from commercial suppliers without any further purification.

### 2.1 | Preparation of Azodye Ligand ( $H_2L$ )

The new azodye ligand  $H_2L$  (Figure 1) was prepared as described previously.<sup>[23]</sup> In short, a suspension of 4-amino-*N*-(4-methylpyrimidin-2-yl)benzenesulfonamide (0.2643 g, 1 mmol) in water (15 ml) and HCl (15 ml) was warmed to 75 °C until entire dissolution. The obtained pure aqueous solution was diazotized below 5 °C with aqueous sodium nitrite (1.5 g in 25 ml of water). To a solution of 2,4-dihydroxybenzaldehyde (0.1381 g, 1 mmol) in water containing 1.6 g of NaOH, the resulting diazonium chloride solution was added dropwise with continuous stirring in the course of 30 min at least. This mixture was stirred for 1 h at 0–5 °C,

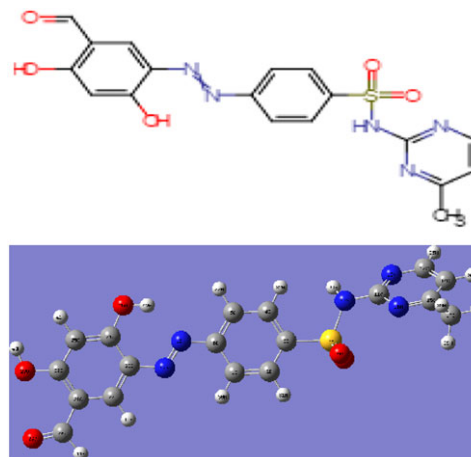


FIGURE 1 Optimized structure of 4-(2,4-dihydroxy-5-formylphen-1-ylazo)-*N*-(4-methylpyrimidin-2-yl)benzenesulfonamide ( $H_2L$ )

and left in a refrigerator for 6 h. The obtained solid product was filtrated off, washed several times with NaCl solution (30 ml, 10%), air-dried and recrystallized several times from hot ethanol.

### 2.2 | Synthesis of Metal Ion Complexes

New metal ion complexes were synthesized by addition of 1 mmol of a methanolic solution of each metal salt (0.4040 g of  $Fe(NO_3)_3 \cdot 9H_2O$ , 0.4002 g of  $Cr(NO_3)_3 \cdot 9H_2O$ , 0.1833 g of  $CdCl_2$ , 0.1979 g of  $MnCl_2 \cdot 4H_2O$ , 0.2377 g of  $NiCl_2 \cdot 6H_2O$ , 0.1705 g of  $CuCl_2 \cdot 2H_2O$ , 0.2195 g of  $Zn(CH_3COO)_2 \cdot 2H_2O$  and 0.2379 g of  $CoCl_2 \cdot 6H_2O$ ) to 1 mmol of  $H_2L$  (0.3974 g) dissolved in MeOH–dimethylformamide (DMF) mixture (20% v/v). The addition process was carried out dropwise with continuous stirring. The obtained reaction mixture was allowed to reflux for 12–15 h over a water bath at a suitable temperature. A few drops of triethylamine were added as basic medium until the formed coloured metal complexes were precipitated. The resulting precipitates were filtered off, washed with ethanol and then desiccated under anhydrous  $CaCl_2$ . The purities of all studied compounds were checked using TLC and melting point constancy.

### 2.3 | Measurements and Instrumentation

Micro-analysis (C, H, N) was carried out at the Micro Analytical Center, Cairo University using a PerkinElmer 2400 CHN elemental analyser. Fourier transform infrared (FT-IR) spectra were obtained using a Bruker Tensor 27 FT-IR spectrophotometer within the range 200–4000  $cm^{-1}$  as KBr discs. Electronic spectra were obtained using a Jenway 6405 spectrophotometer in dimethylsulfoxide (DMSO) as a solvent in the range 200–900 nm. Room temperature electron spin resonance (ESR) spectra were recorded with a Jeol JES-RE1X EPR spectrometer applying DPPH as

TABLE 1 Microanalysis, physical characteristics and molar conductance data of investigated sulfa drug complexes<sup>a</sup>

Molecular formula; empirical formula	Molecular weight, found (calcd)	Colour ( $\Lambda_m$ )	Microanalysis, found (calcd)		
			C (%)	H (%)	N (%)
H <sub>2</sub> L (C <sub>18</sub> H <sub>15</sub> N <sub>5</sub> O <sub>5</sub> S)	413.00(413.41)	Yellowish orange(—)	52.28(52.30)	3.66(3.66)	16.90 (16.94)
1) [FeHL(NO <sub>3</sub> ) <sub>2</sub> (CH <sub>3</sub> OH) <sub>2</sub> ]; C <sub>20</sub> H <sub>22</sub> FeN <sub>7</sub> O <sub>13</sub> S	656.00(656.34)	Deep brown(10.23)	36.31(36.60)	3.76(3.38)	— (14.94)
2) [CrHL(NO <sub>3</sub> ) <sub>2</sub> (H <sub>2</sub> O)(CH <sub>3</sub> OH)]; C <sub>19</sub> H <sub>20</sub> CrN <sub>7</sub> O <sub>13</sub> S	638.00(638.46)	Faint brown(10.55)	35.43(35.74)	3.63(3.16)	— (15.36)
3) [CdHLCI(H <sub>2</sub> O)] <sub>2</sub> H <sub>2</sub> O; C <sub>18</sub> H <sub>20</sub> CdClN <sub>5</sub> O <sub>8</sub> S	614.00(614.31)	Brown(9.88)	35.78(35.19)	3.26(3.28)	11.54(11.40)
4) [MnHLCI(H <sub>2</sub> O) <sub>3</sub> ]; C <sub>18</sub> H <sub>20</sub> ClMnN <sub>5</sub> O <sub>8</sub> S	—(556.84)	Deep brown(9.36)	38.46(38.82)	3.00(3.62)	12.13(12.58)
5) [NiHLCI(H <sub>2</sub> O) <sub>3</sub> ]; C <sub>18</sub> H <sub>20</sub> ClN <sub>5</sub> NiO <sub>8</sub> S	560.00(560.59)	Dark green(8.42)	38.14(38.57)	3.28(3.60)	12.14(12.49)
6) [CuHLCI(H <sub>2</sub> O)]; C <sub>18</sub> H <sub>16</sub> ClCuN <sub>5</sub> O <sub>6</sub> S	529.00(529.41)	Brown(8.76)	40.48(40.84)	3.19(3.05)	12.59(13.23)
7) [ZnHL(CH <sub>3</sub> COO)(H <sub>2</sub> O)]; C <sub>20</sub> H <sub>19</sub> N <sub>5</sub> O <sub>8</sub> SZn	554.00(554.85)	Reddish brown(9.12)	38.33(38.29)	3.13(3.45)	12.60(12.62)
8) [CoHLCI(H <sub>2</sub> O)] <sub>2</sub> H <sub>2</sub> O; C <sub>18</sub> H <sub>18</sub> ClCoN <sub>5</sub> O <sub>7</sub> S	542.00(542.82)	Dark green(8.94)	40.66(39.83)	3.59(3.34)	12.46(12.90)

<sup>a</sup>The yield for the synthesized complexes was found to be 77.35–80.42%; molecular weight was obtained from mass spectra; and  $\Lambda_m$  is the molar conductance ( $\Omega^{-1} \text{ cm}^2 \text{ mol}^{-1}$ ) at room temperature.

an external standard. The effective magnetic moments were estimated at ambient temperature using a Johnson Matthey magnetic susceptibility balance. The molar conductance of the studied metal chelates was obtained using a Jenway model 4070 conductance bridge. A Shimadzu GV-5050 mass spectrometer was used to measure the electron ionization mass spectra (EI-MS) of all compounds using the electron spray ionization technique. X-ray diffraction (XRD) patterns were measured with an X-ray diffractometer (GNR, APD2000PRO, Italy) with a graphite monochromator using Cu  $K\alpha_1$  radiation at  $0.03^\circ \text{ min}^{-1}$  scanning rate. Using Joel JSM-6390 equipment, transmittance electron microscopy (TEM) images were obtained. Thermogravimetric analysis (TGA) was performed with a Shimadzu TGA-50 thermal analyser under dynamic nitrogen atmosphere with a heating rate of  $10^\circ \text{ C min}^{-1}$  from ambient temperature up to  $800^\circ \text{ C}$ . Antibacterial and antifungal activities of the synthesized compounds were investigated using the agar well diffusion method.<sup>[24]</sup> The anticancer activity of the free ligand and complexes was studied towards human liver carcinoma (HEPG2) cell line at the Regional Center for Microbiology and Biotechnology, Al-Azhar University as well as other biological activities.<sup>[25,26]</sup>

## 2.4 | Theoretical Aspects

### 2.4.1 | Structural optimization

In the gas phase, the best orientations of sulfa drug ligand structure and its eight complexes were accomplished using Gaussian09 software.<sup>[27]</sup> Density functional theory (DFT)/B3LYP is the best method for achieving the optimization using different base sets. The output Gaussian files were viewed using visualization screen in the program.<sup>[28]</sup> Essential parameters abstracted were on the bases of frontier orbital energy values. Other essential data were obtained from output log file: oscillator strength, excitation energy and bond lengths and charges attributed to coordinating centres. A quantitative structure–activity relationship (QSAR) study was accomplished for the organic compound to give a general overview of its stability and biological activities.

### 2.4.2 | Docking implementation

Applying Autodock Tools 4.2 was achieved by using Gasteiger partial charges which were added to sulfa drug atoms. The docked protein receptor complexes were executed using integrated non-polar hydrogen atoms and rotatable bonds were refined. Running of the program began with the

TABLE 2 Assignments for diagnostic important bands in FT-IR spectra of H<sub>2</sub>L and its complexes

Compound	$\nu(\text{OH})$	$\nu(\text{NH})$	$\nu(\text{C}=\text{N})$	$\nu(\text{N}=\text{N})$	$\delta(\text{H}_2\text{O})$	$\nu(\text{M}-\text{O})$	$\nu(\text{M}-\text{N})$	$\nu(\text{M}-\text{Cl})$
H <sub>2</sub> L	3421	2925	1478	1407	—	—	—	—
1	3421	2939	1476	1389	803	601	475	—
2	3423	2937	1477	1385	803	577	460	—
3	3444	2929	1452	1411	797	600	452	369
4	3413	2931	1486	1411	802	590	482	374
5	3419	2933	1491	1412	802	612	484	364
6	3446	2920	1472	1365	794	607	453	317
7	3418	2929	1469	1380	805	605	410	—
8	3416	2947	1456	1410	797	611	484	364

TABLE 3 Electronic spectral data for metal ion–sulfa drug complexes

Compound	$\mu_{\text{eff}}$ (BM)	D–d transition( $\text{cm}^{-1}$ )	Intraligand and charge transfer ( $\text{cm}^{-1}$ )	Ligand field parameters			
				10Dq ( $\text{cm}^{-1}$ )	$B$ ( $\text{cm}^{-1}$ )	$\beta$	$Z$
H <sub>2</sub> L	—	—	35 843; 31 824; 28 420; 21 400	—	—	—	—
1	5.62	27 560; 21 100; 20 833	34 735; 31 056	20 833	868.04	0.8552	2.011
2	3.81	20 661; 14 648	33 860; 29 239	14 648	606.70	0.6609	1.292
3	dia	—	34 650; 33 014; 27 472; 21 930	—	—	—	—
4	5.93	18 240; 21 645; 27 473	34 000	18 240	760.00	0.8837	1.4622
5	3.11	25 727; 15 949	32 679; 27 778	10 034.5	771.89	0.7415	0.8024
6	1.65	20 325	33 333; 25 381; 22 321	—	—	—	—
7	dia	—	31 646; 26 042; 22 321; 17 730	—	—	—	—
8	4.61	16 541	32 258; 25 125; 22 624	3 723.57	789.81	0.8134	1.0861

addition of fundamental hydrogen atoms and Kollman united atom type charges.<sup>[29]</sup> Autogrid program was implemented to produce the affinity (grid) maps of  $\times \times \text{Å}$  grid points and 0.375 Å spacing.<sup>[30]</sup> Electrostatic terms and van der Waals forces were evaluated through distance-dependent dielectric functions and Autodock parameter sets, respectively. Docking simulations were accomplished by the local search method of Solis and Wets and Lamarckian genetic algorithm.<sup>[31]</sup> Occasionally, initial position, orientation and torsions of the drug molecule were set. All rotatable torsions were released during docking. Ten different runs were used to achieve each docking experiment, that were set to block after an ultimate 250 000 energy consideration. The size was established to be 150. Throughout the study, a translational step of 0.2 Å, quaternion and torsion steps of five were used.

### 3 | RESULTS AND DISCUSSION

The new azodye ligand H<sub>2</sub>L and its metal ion complexes (1–8) are found to be stable towards moisture, light and air. The coloured ligand is soluble in polar organic solvents such as ethanol and methanol in the presence of DMF solvent. The eight coloured complexes are soluble in DMF and DMSO but are insoluble in other common organic solvents. The micro-analyses confirm that the complexes have a metal-to-ligand molar ratio of 1:1. The obtained results of micro-analyses are consistent with the calculated results from empirical formulae of all complexes (Table 1). The molar conductance values of the complexes lie within the range 8.42–10.55  $\Omega^{-1} \text{cm}^2 \text{mol}^{-1}$  which indicates that these mononuclear complexes are non-electrolytes.<sup>[32]</sup>

#### 3.1 | FT-IR Spectra and Mode of Bonding

The FT-IR spectral bands of diagnostic importance for the drug derivative and its metal chelates are presented in Table 2. The binding coordination modes for the ligand towards metal ions were scrutinized by comparing the FT-IR

spectrum of the free ligand with those of its metal complexes. The spectrum of the ligand displays a broad band centred at 3421  $\text{cm}^{-1}$  attributed to stretching vibrations of intramolecular hydrogen bonded hydroxyl groups.<sup>[33]</sup> Spectra of complexes show broad bands in the range 3413–3446  $\text{cm}^{-1}$  corresponding to  $\nu_{\text{OH}}$  of solvent molecules associated with the complexes. Also, the complexes exhibit weak bands at 794–805  $\text{cm}^{-1}$  for  $\delta_{\text{r}}(\text{H}_2\text{O})$  of coordinated molecules.<sup>[34]</sup> Moreover, fresh bands at 1090, 1275  $\text{cm}^{-1}$  and 1090, 1317  $\text{cm}^{-1}$  for  $\nu(\text{M}-\text{OH})$  and  $\delta(\text{OH})$  are good indications for the presence of CH<sub>3</sub>OH molecules associated with Fe(III) and Cr(III) complexes, respectively. The behaviour of OH groups in the drug cannot be detected from their stretching and bending vibrations in the spectra of the complexes due to their replacement by the same from solvents. The band appearing at 1407  $\text{cm}^{-1}$  assigned to  $\nu_{\text{N}=\text{N}}$  is shifted upon chelate formation denoting its coordination towards

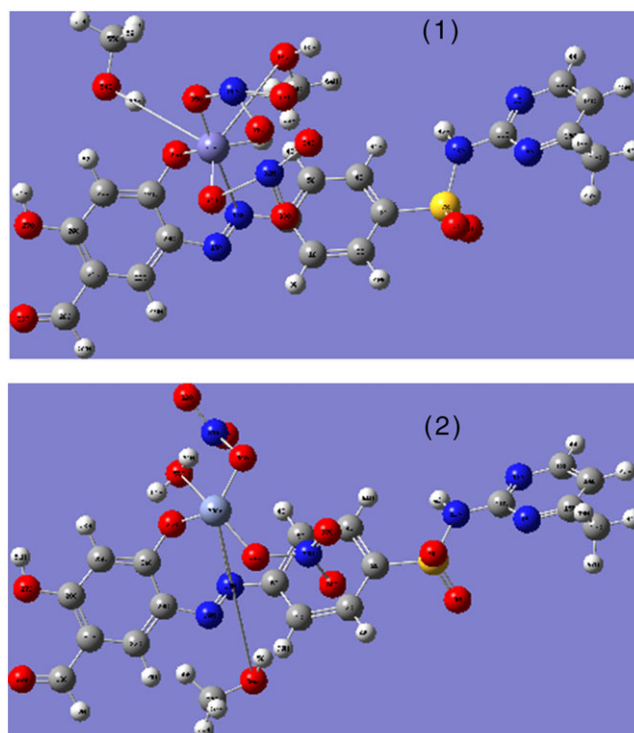


FIGURE 2 Optimized structural formulae for Fe(III) and Cr(III) complexes

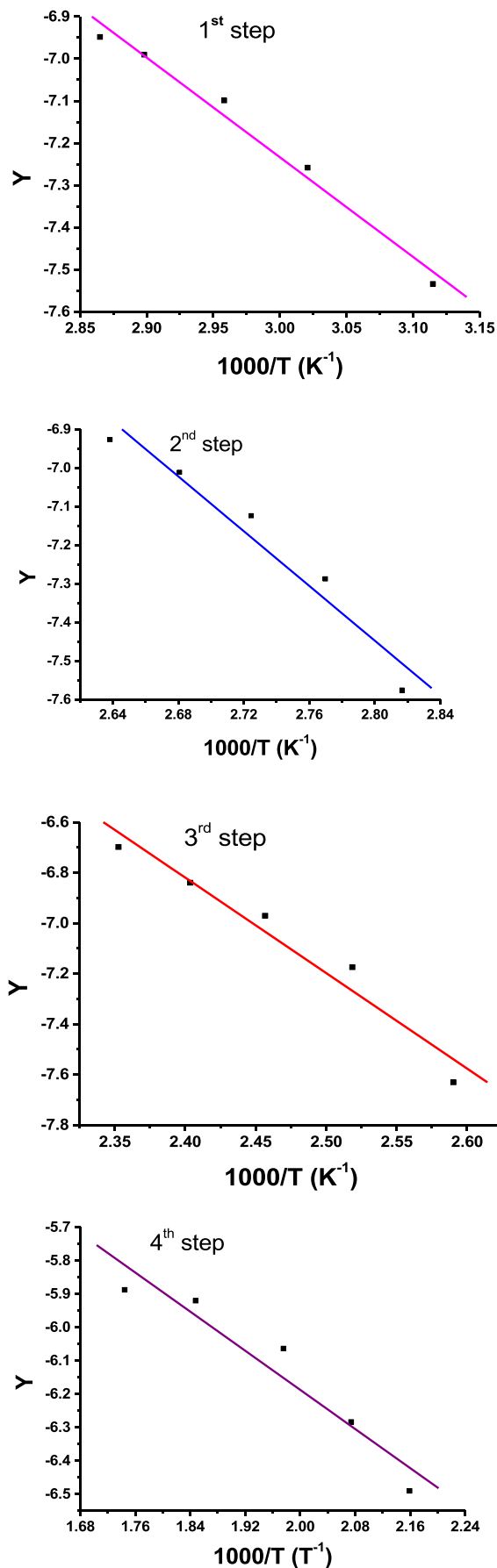


FIGURE 3 Coats-Redfern plots for  $[\text{CoLCI}(\text{H}_2\text{O})]\text{H}_2\text{O}$  (8).  $Y = \log[-\log(1 - \alpha)/T^2]$ , where  $\alpha$  is the fraction decomposed and  $T$  is the absolute temperature;  $n = 1$  for the distinct thermal degradation steps

metal centres. In most cases,  $\nu_{\text{NH}}$ ,  $\nu_{\text{C=O}}$  and  $\nu_{\text{C=N}}$  of pyrimidine ring and  $\nu_{\text{SO}_2(\text{sym})}$  bands appearing at 2925, 1625, 1478 and 1148  $\text{cm}^{-1}$  in the drug spectrum manifest slight shifts in spectra of the complexes. This rules out such groups from participation in chelation with metal centres. The spectra include the occurrence of new bands at 577–612 and 410–484  $\text{cm}^{-1}$  assigned to M–O and M–N stretching, respectively.<sup>[35]</sup> This confirms the coordination of one nitrogen atom from azo group and ionized *o*-hydroxyl group towards all central metal atoms. The  $\nu(\text{M–Cl})$  band appears in the lower frequency range up to 374  $\text{cm}^{-1}$  in the spectra of the complexes.<sup>[36]</sup> Furthermore, for Fe(III) and Cr(III) chelates (**1** and **2**), the appearance of two bands at 1436, 1234  $\text{cm}^{-1}$  and 1432, 1236  $\text{cm}^{-1}$ , respectively, with a difference  $\Delta = 202$  and 196  $\text{cm}^{-1}$  indicates the coordination of nitrate group in monodentate mode.<sup>[34]</sup> Also, for Zn(II) complex (**7**), the appearance of  $\nu_{\text{as}}(\text{OCO})$  and  $\nu_{\text{s}}(\text{OCO})$  bands at 1660 and 1432  $\text{cm}^{-1}$ , respectively, confirms the unidentate mode of acetate group.<sup>[34]</sup>

### 3.2 | Electronic Spectral Analysis

Essential spectral analysis data are summarized in Table 3, obtained after the exposure of solvated compounds to a wide range of wavelengths (200–900 nm). Magnetic moment values (Table 3) were also calculated to establish a detailed view on the structural formulae. Free drug spectrum displays observable intraligand transition bands at 35 843 and 31 824  $\text{cm}^{-1}$  for  $\pi \rightarrow \pi^*$  and 28 420 and 21 400  $\text{cm}^{-1}$  for  $n \rightarrow \pi^*$  transitions. The value of molar absorptivity (for 1.05  $\text{mmol l}^{-1}$ ) assigned to  $n \rightarrow \pi^*$  transition is  $\epsilon_1 = 214 \text{ mol}^{-1} \text{ dm}^3 \text{ cm}^{-1}$  which is applicable for the first transition (HOMO  $\rightarrow$  LUMO). A distinct conjugation for enriched chromophor groups spread along the drug structure is the main cause for redshift of charge transfer (CT) bands. The spectrum of the  $[\text{FeHL}(\text{NO}_3)_2(\text{CH}_3\text{OH})_2]$  complex (**1**) exhibits three significant d–d transition bands at 27 560, 21 100 and 20 833  $\text{cm}^{-1}$ . Such bands belong to  ${}^6\text{A}_{1\text{g}} \rightarrow {}^4\text{E}_{\text{g}}$ ,  ${}^4\text{A}_{1\text{g}}(\text{G}, \nu_3)$ ,  ${}^6\text{A}_{1\text{g}} \rightarrow {}^4\text{T}_{2\text{g}}(\text{G}, \nu_2)$  and  ${}^6\text{A}_{1\text{g}} \rightarrow {}^4\text{T}_{1\text{g}}(\text{G}, \nu_1)$  transitions, respectively, inside an octahedral configuration (Figure 2). Its magnetic susceptibility value (5.62 BM) agrees comfortably with high-spin octahedral feature. Values of 10Dq, Racah and nephelauxetic parameters (20 833  $\text{cm}^{-1}$ , 868.04  $\text{cm}^{-1}$  and 0.8552) were computed. Nephelauxetic parameter reflects highly ionic nature of Fe–L bonds. The spectrum of the  $[\text{CrHL}(\text{NO}_3)_2(\text{H}_2\text{O})(\text{CH}_3\text{OH})]$  complex (**2**) exhibits two significant transition bands at 20 661 and 14 648  $\text{cm}^{-1}$ . Such bands belong to  ${}^4\text{A}_{2\text{g}}(\text{F}) \rightarrow {}^4\text{T}_{1\text{g}}(\text{F})(\nu_2)$  and  ${}^4\text{A}_{2\text{g}} \rightarrow {}^4\text{T}_{2\text{g}}(\text{F})(\nu_1)$  transitions, respectively, inside an octahedral configuration (Figure 2). Its magnetic moment value (3.81 BM) coincides well with spin-only moment, which rules out the orbital contribution for  $d^3$  systems. Racah parameter value (606.70  $\text{cm}^{-1}$ ) was calculated using the standard equation.<sup>[37]</sup> Nephelauxetic parameter value (0.6609) obtained by applying the relation  $\beta = B(\text{complex})/$

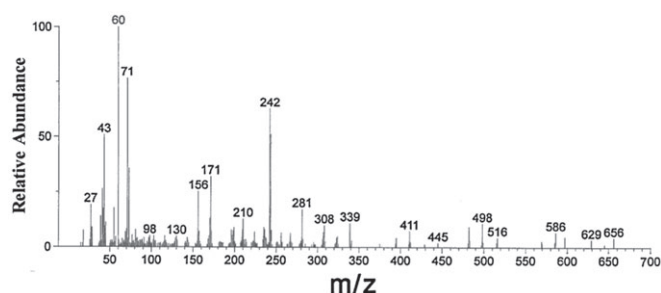
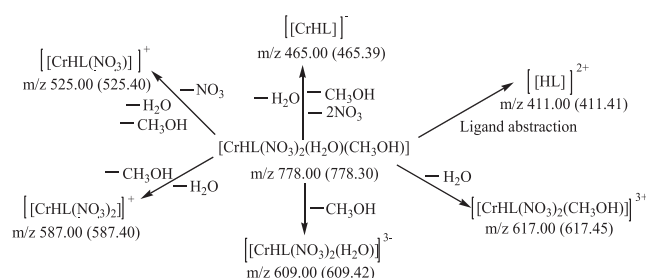
TABLE 4 Coats–Redfern thermodynamic parameters for some metal complexes<sup>a</sup>

Compound	n	Step	r	T (K)	E* (kJ mol <sup>-1</sup> )	H* (kJ mol <sup>-1</sup> )	ln A	S* (kJ mol <sup>-1</sup> K <sup>-1</sup> )	G* (kJ mol <sup>-1</sup> )
1	1	1st	0.9509	410	0.0108	-3.3980	-8.3014	-0.3249	129.8086
	1	2nd	0.9970	574	0.0306	-4.7417	2.1950	-0.2404	133.2619
	1	3rd	0.9941	735	0.1081	-6.0027	-8.9623	-0.3352	240.4002
2	1	1st	0.9915	339	0.0566	-2.7619	-8.3014	-0.3233	106.8413
	1	2nd	0.9306	396	0.0300	-3.2623	2.1950	-0.2373	90.7236
	1	3rd	0.9887	561	0.0330	-4.6312	-8.9623	-0.3330	182.1795
4	0	1st	0.9702	406	0.0169	-3.3586	-8.3014	-0.3248	128.5153
	1	2nd	0.9615	473	0.2223	-3.7102	2.1950	-0.2388	109.2494
	0	3rd	0.9918	605	0.0055	-5.0245	-8.9623	-0.3336	196.8178
5	0	1st	0.9304	498	0.0204	-4.1200	-8.3014	-0.3265	158.4823
	1	2nd	0.9677	580	0.2066	-4.6155	2.195013	-0.2405	134.8808
	1	3rd	0.9941	832	0.0432	-6.8741	-8.9623	-0.3363	272.9047
7	1	1st	0.9773	500	0.0112	-4.1458	-8.3014	-0.3265	159.1263
	1	2nd	0.9835	575	0.1647	-4.6158	2.1950	-0.2404	133.6365
	0	3rd	0.9565	741	0.0261	-6.1346	-8.9623	-0.3353	242.3298
8	1	1st	0.9914	335	0.0453	-2.7399	-8.3014	-0.3232	105.5369
	1	2nd	0.9738	367	0.0679	-2.9834	2.1950	-0.2367	83.8877
	1	3rd	0.9765	406	0.0724	-3.3031	-8.9623	-0.3303	130.8018
	1	4th	0.9603	518	0.0281	-4.2786	-9.5646	-0.3373	170.4637

<sup>a</sup>A is the frequency factor, E is the activation energy,  $\Delta H^*$  is the activation enthalpy,  $\Delta S^*$  is the activation entropy and  $\Delta G^*$  is the Gibbs free energy.

$B^0$  (free ion) is attributed to low-energy quartet–doublet transitions. This value reflects the relative covalent character for new  $\sigma$  bonds coincident with Cr–O and Cr–N interactions.<sup>[38]</sup> Spectra of  $[\text{CdHLCl}(\text{H}_2\text{O})]2\text{H}_2\text{O}$  (**3**) and  $[\text{ZnHL}(\text{CH}_3\text{COO})(\text{H}_2\text{O})]$  (**7**) exhibit CT bands attributed to diamagnetic complexes with tetrahedral configuration. The deep colour of the two complexes, although the absence of d–d electronic transitions, reflects the dominant ligand-to-metal CT. The spectrum of  $[\text{MnHLCl}(\text{H}_2\text{O})_3]$  (**4**) exhibits three transition bands at 27 473, 21 645 and 18 240  $\text{cm}^{-1}$ . Such bands are assigned to  ${}^6\text{A}_{1g} \rightarrow {}^4\text{E}_g$ ,  ${}^4\text{A}_{1g}(\text{G}, \nu_3)$ ,  ${}^6\text{A}_{1g} \rightarrow {}^4\text{T}_{2g}(\text{G}, \nu_2)$  and  ${}^6\text{A}_{1g} \rightarrow {}^4\text{T}_{1g}(\text{G}, \nu_1)$  transitions, respectively, inside an octahedral configuration. Its magnetic moment value (5.93 BM) coincides well with spin-only moment expected for low-field  $d^5$  complexes. Values of 10Dq, Racah and nephelauxetic parameters (18 240  $\text{cm}^{-1}$ , 760  $\text{cm}^{-1}$  and 0.8837) were computed and indicate the absence of elemental feature with considerable ionic character for new  $\sigma$  bonds. The spectrum of  $[\text{NiHLCl}(\text{H}_2\text{O})_3]$  (**5**) exhibits two significant d–d transition bands at 25 727 and 15 949  $\text{cm}^{-1}$  assigned to  ${}^3\text{A}_{2g} \rightarrow {}^3\text{T}_{1g}(\text{p})(\nu_3)$  and  ${}^3\text{A}_{2g} \rightarrow {}^3\text{T}_{1g}(\text{F})(\nu_2)$  transitions, respectively.<sup>[39]</sup> Its magnetic moment value (3.11 BM) agrees with spin-only moment for  $d^8$  system. Values of 10Dq, Racah and nephelauxetic

parameters (10 034.5  $\text{cm}^{-1}$ , 771.89  $\text{cm}^{-1}$  and 0.7415) were computed and represent also the ionic nature for new  $\sigma$  bonds. The spectrum of  $[\text{CuHLCl}(\text{H}_2\text{O})]$  (**6**) exhibits a significant band at 20 325  $\text{cm}^{-1}$  assigned to  ${}^2\text{B}_{1g} \rightarrow {}^2\text{E}_g$  transition inside a square planar configuration. Its magnetic moment value (1.65 BM) coincides with spin of free electron with a relative metal–metal interaction inside the crystal. Also, the band at 22 321  $\text{cm}^{-1}$  is attributed to ligand-to-metal CT. The spectrum of  $[\text{CoHLCl}(\text{H}_2\text{O})]2\text{H}_2\text{O}$  (**8**) exhibits one significant band at 16 541  $\text{cm}^{-1}$  assigned to  ${}^4\text{A}_2(\text{F}) \rightarrow {}^4\text{T}_1(\text{P})$  transition inside a tetrahedral configuration (Figure 1S). Its magnetic moment value (4.61 BM) is in the range suitable for the appearance of orbital contribution inside a tetrahedral configuration. Values of 10Dq, Racah and nephelauxetic parameters (3723.57  $\text{cm}^{-1}$ , 789.81  $\text{cm}^{-1}$  and 0.8134) were computed<sup>[40]</sup> and indicate a considerable ionic character for new  $\sigma$  bonds. Values of Racah inter-electronic repulsion parameter are changed with 3d transition metal complexes by changing Z and q values, where Z is the cation charge efficiency and q is the number of existing d-shell as  $d^q$ . The effective metallic charges are computed using a known relation<sup>[40]</sup> and found as +2.011, +1.292, +1.4622, +0.8024 and +1.0861 for Fe(III), Cr(II), Mn(II), Ni(II) and Co(II) ions, respectively.<sup>[40]</sup> These values are frequently

FIGURE 4 Mass spectrum of  $[\text{FeHL}(\text{NO}_3)_2(\text{CH}_3\text{OH})_2]$  (**1**)SCHEME 1 Fragmentation pathways of  $[\text{CrHL}(\text{NO}_3)_2(\text{H}_2\text{O})(\text{CH}_3\text{OH})]$  (**2**)

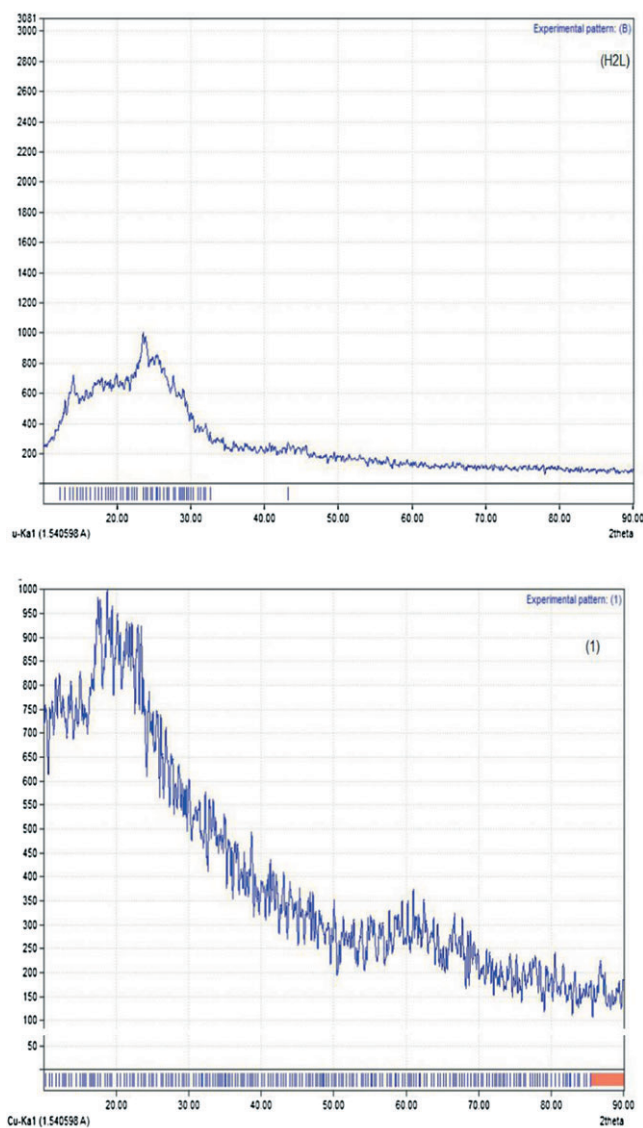


FIGURE 5 XRD patterns for H<sub>2</sub>L and Fe(III) complex

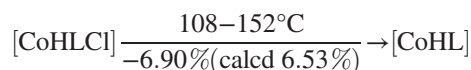
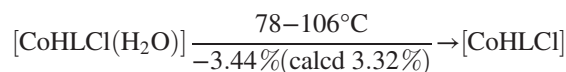
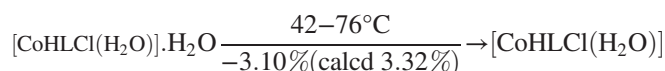
below that of the formal charges. This reduction for oxidation states is indicative of the effective ionic nature for new  $\sigma$  bonds covered with high ligand-to-metal CT.<sup>[41]</sup>

### 3.3 | TGA and Thermo-kinetic Parameters

Most of the investigated metal complexes were subjected to TGA in order to understand their coordination structure.<sup>[42,43]</sup>

The TGA curve of Fe(III) complex (1) exhibits three pyrolysis processes. The first mass loss occurs in the range 53–200 °C, corresponding to the removal of two coordinated methanol molecules. The found mass loss (10.00%) is close to the calculated value (9.76%). The second pyrolysis step takes place within the range 204–370 °C attributed to the

release of two nitrate groups with 18.87% (calcd 18.89%) mass loss. The last degradation stage happens at 372–1000 °C involving complete decomposition of the complex and formation of Fe<sub>2</sub>O<sub>3</sub> (12.59%; calcd 12.17%) as the residue. For [CrHL(NO<sub>3</sub>)<sub>2</sub>(H<sub>2</sub>O)(CH<sub>3</sub>OH)] (2), the first step appears at 48–78 °C attributed to the volatilization of coordinated solvent molecules (H<sub>2</sub>O + CH<sub>3</sub>OH) with 7.69% (calcd 7.84%) mass loss. The second step occurs at 80–154 °C attributed to removal of two coordinated nitrate groups with 19.23% (calcd 19.42%) mass loss. The composition of the final residue is Cr<sub>2</sub>O<sub>3</sub> + 5C, and the experimental result (21.54%) is in good agreement with the result of theoretical calculation (21.30%). [CuHLCl(H<sub>2</sub>O)] (6) shows a first decomposition stage at 272–302 °C assignable to the removal of coordinated water with 3.33% (calcd 3.40%) mass loss. The next thermal decomposition step at 304–322 °C is attributed to elimination of 0.5Cl<sub>2</sub> with 6.82% (calcd 6.70%) mass loss. The final step at 324–984 °C involves thermal degradation of the complex leaving Cu metal as final residual component with 11.96% (calcd 12.00%). [ZnHL(CH<sub>3</sub>COO)(H<sub>2</sub>O)] (7) displays three successive thermal degradation stages. The first one at 148–276 °C is assigned to the liberation of one coordinated water molecule with 3.34% (calcd 3.25%) mass loss. The second step at 278–316 °C corresponds to the elimination of coordinated acetate with 10.83% (calcd 10.64%) mass loss. The third one at 318–598 °C corresponds to the thermal decomposition of the complex and formation of Zn as a metallic residue,<sup>[44]</sup> amounting to 10.05% (calcd 11.79%). [CoHLCl(H<sub>2</sub>O)]H<sub>2</sub>O (8) degrades in four consecutive thermal decomposition steps in the following mechanism:



TGA curves were applied to calculate the kinetic parameters applying the Coats–Redfern method<sup>[45]</sup> (Figure 3). Also, the thermodynamic parameters of the thermal decomposition stages were determined<sup>[46]</sup> (Table 4). The negative

TABLE 5 Spin Hamiltonian parameters for Cu(II) complex ( $A$  and  $p \times 10^{-4}$ )

Complex	$g_{\parallel}$	$g_{\perp}$	$g_0$	$A_{\parallel}$	$f$	$A_{\perp}$	$A_0$	$G$	$p$	$k$	${}^2K_{\parallel}$	${}^2K_{\perp}$	$\alpha^2$	$\beta^2$
3	2.1606	2.0935	2.116	163.12	132.45	63.31	96.58	1.74	25.55	3.894	-0.484	-1.114	0.691	0.703

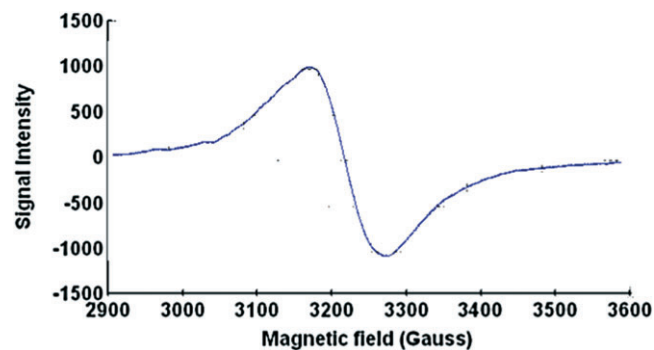


FIGURE 6 ESR spectrum of solid Cu(II) complex

sign of all  $\Delta H^*$  values reveals that all thermal decomposition stages are exothermic. The activation entropies ( $\Delta S^*$ ) have negative values which donate a more ordered activated complex than the reactants and/or the thermal degradation processes are slower than normal ones.<sup>[47]</sup>  $\Delta G^*$  values increase in an adequately behavior for the subsequent thermal decomposition steps as a result of increasing  $T\Delta S^*$  values from one step to upcoming ones overriding  $\Delta H^*$  values.<sup>[48]</sup>  $\Delta S^*$  of the dehydration step has small negative values because this step includes two simultaneous processes. The first is release of water molecules from the solid complex with positive  $\Delta S^*$  and the second is the formation of anhydrous complexes (more ordered) with negative  $\Delta S^*$ . The obtained values are the resultant of both processes.<sup>[49]</sup>

### 3.4 | Mass Spectral Analysis

EI-MS analysis was applied in order to support the constituents and purities of the prepared ligand and metal complexes (Figure 2S). Mass spectra of free drug ( $H_2L$ ),  $[FeHL(NO_3)_2(CH_3OH)_2]$  (Figure 4),  $[CrHL(NO_3)_2(H_2O)(CH_3OH)]$ ,  $[CdHLCl(H_2O)]_2H_2O$ ,  $[NiHLCl(H_2O)_3]$ ,  $[CuHLCl(H_2O)]$ ,  $[ZnHL(CH_3COO)(H_2O)]$  and  $[CoHLCl(H_2O)]H_2O$  display peaks at  $m/z$  413, 656, 638, 614, 560, 529, 554 and 542, respectively, consistent with their molecular weights. Furthermore, most of the studied

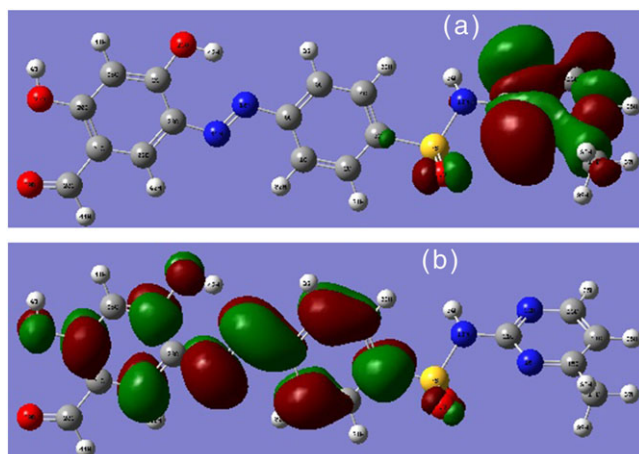


FIGURE 7 Frontier molecular orbitals of (A) HOMO and (B) LUMO

complexes degrade through the elimination of drug ligand which gives rise to the occurrence of molecular ion peaks assignable to  $[L]^+$  besides other peaks due to successive fragmentation processes of the complexes. This is a very widespread behaviour for metal ion complexes containing distinct ligands (ML) which decompose during spray ionization processes via cleavage of the metal–ligand bonds.<sup>[50,51]</sup> As example, the mass spectrum of complex **2** displays molecular ion peaks at  $m/z$  638, 609, 617, 587, 525, 465 and 411

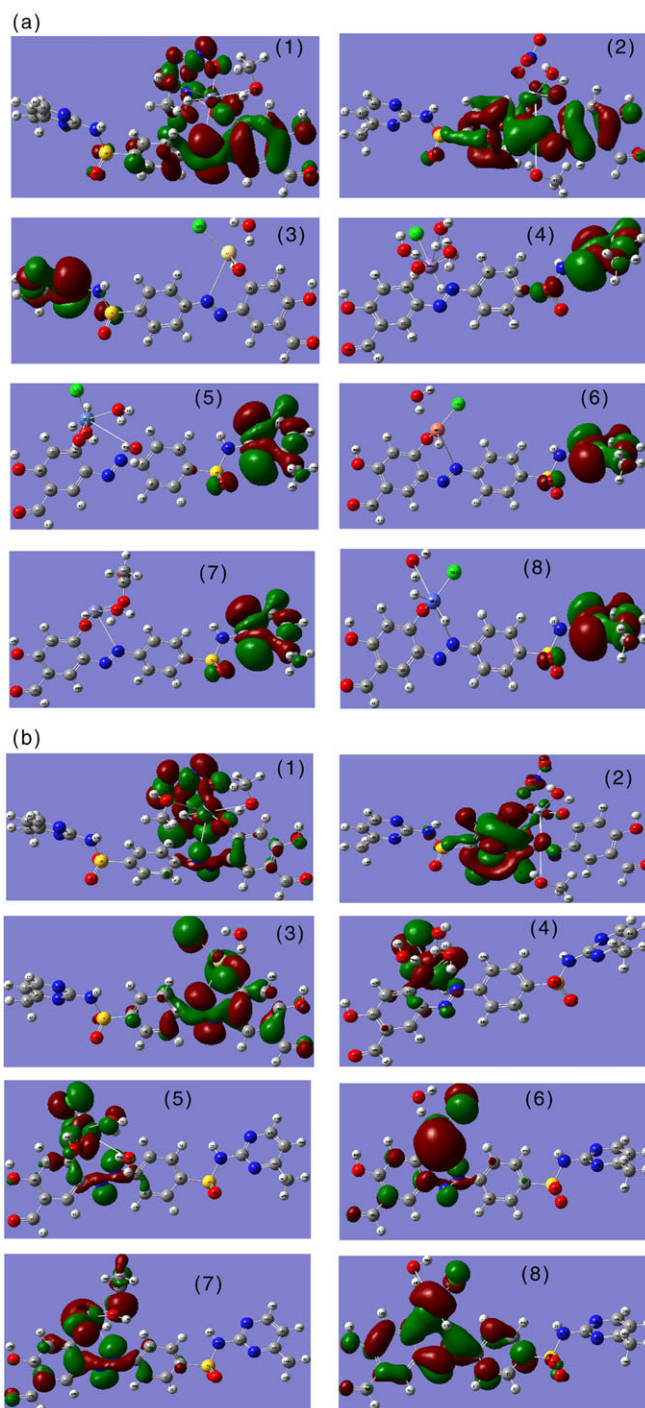


FIGURE 8 Frontier molecular orbitals of (A) HOMO and (B) LUMO for Fe(III), Cr(III), Cd(II), Mn(II), Ni(II), Cu(II), Zn(II) and Co(II) complexes (1–8, respectively)

TABLE 6 Gaussian optimized parameters using DFT/B3LYP method

Compound	$E_H$ (eV)	EL (eV)	(EH – EL) (eV)	EI – Eh	$x$ (eV)	$\mu$ (eV)	$\eta$ (eV)	$S$ (eV <sup>-1</sup> )	$\omega$ (eV)	(eV)
H <sub>2</sub> L	-0.2430	-0.11654	-0.1265	0.12646	0.17977	-0.17977	0.06323	0.031615	0.255553	15.81527756
Fe(III)–HL	-0.23194	-0.20994	-0.0220	0.02200	0.22094	-0.22094	0.0110	0.00550	2.21884	90.90909091
Cr(III)–HL	-0.20767	-0.14533	-0.0623	0.06234	0.17650	-0.1765	0.03117	0.015585	0.499715	32.08213025
Cd(II)–HL	-0.23793	-0.14656	-0.0914	0.09137	0.192245	-0.19225	0.045685	0.022843	0.404489	21.88902266
Mn(II)–HL	-0.23254	-0.19226	-0.0403	0.04028	0.21240	-0.2124	0.02014	0.010070	1.120004	49.65243297
Ni(II)–HL	-0.23577	-0.21992	-0.0159	0.01585	0.227845	-0.22785	0.007925	0.003963	3.27529	126.1829653
Cu(II)–HL	-0.23636	-0.20011	-0.0363	0.03625	0.218235	-0.21824	0.018125	0.009062	1.313835	55.17241379
Zn(II)–HL	-0.23394	-0.12787	-0.1061	0.10607	0.180905	-0.18091	0.053035	0.026518	0.308538	18.8554728
Co(II)–HL	-0.23701	-0.1950	-0.0420	0.04201	0.216005	-0.21601	0.021005	0.010503	1.110644	47.60771245

corresponding to [CrHL(NO<sub>3</sub>)<sub>2</sub>(H<sub>2</sub>O)(CH<sub>3</sub>OH)] (molecular weight of complex), [CrHL(NO<sub>3</sub>)<sub>2</sub>(H<sub>2</sub>O)]<sup>3-</sup> (loss of coordinated methanol), [CrHL(NO<sub>3</sub>)<sub>2</sub>(CH<sub>3</sub>OH)]<sup>3+</sup> (loss of coordinated water), [CrL(NO<sub>3</sub>)<sub>2</sub>]<sup>+</sup> (loss of methanol and water), [CrHL(NO<sub>3</sub>)]<sup>+</sup>, [CrHL]<sup>-</sup> and [HL]<sup>2+</sup>, respectively (Scheme 1). The results of EI-MS are in good agreement with elemental analyses (Table 1) which confirm the proposed molecular formulae of all investigated compounds.

### 3.5 | XRD and TEM

XRD patterns for all prepared compounds were obtained in the range 10° < 2θ < 80° (Figure 3S). This analysis is used to give a clear view about the lattice dynamics of solid compounds.<sup>[52]</sup> All the patterns obtained reflect the amorphous appearance of the drug (Figure 5) and its complexes. This may be due to there being no regular arrangement for the solid constituents during the precipitation process. Almost any compound may solidify in an amorphous state if the reaction is fast or the solution is cooled rapidly enough. Some solids are intrinsically amorphous, due to their constituents not being able to give a good fit inside a crystalline lattice. This prohibits the chance for computing the crystallite sizes or *d*-spacing inside the lattice to give a distinct view about the investigated compounds. The amorphous nature reflects the infinitely small size for the aggregates which may be found comfortably in the nanometre range which is verified through TEM analysis. TEM is a broadly

implemented method used to investigate the particle shape and size for a solid matrix. High-resolution images were obtained (Figure 4S). The micrographs indicate diverse particle shapes in nanocrystalline matrices. A rocky shape is the main feature for free drug and Zn(II) complex (7). This suggests the adaptable accumulation for the particles. Micrographs of Cd(II), Mn(II) and Cu(II) complexes (3, 4 and 6) represent their nanometric features by clear cubic-like crystal shapes. Micrographs of Fe(III), Cr(III), Ni(II) and Co(II) complexes (1, 2, 5 and 8) display clear homogeneous matrices with a distinct isolation for spherical particles in the nanometre range. This points to essential rule for the presence of metal ions on yielding nanometre particles.<sup>[53]</sup> The highly symmetric spherical anions occluded in complexation sphere may lead to the spherical feature appearing in images. Also, this may be the result of the distinct accumulation of several individual particles of polycrystalline nature. The dark areas in the micrographs may point to the aggregation of condensed fine particles. The nanometre sizes may enhance the biological activity with regard to bulk analogue. This property may simplify the permeability through infected cell membranes.

### 3.6 | ESR Spectrum of Cu(II) Complex

Spin Hamiltonian operators and interaction exchange vector (*G*) for solid Cu(II) complex were estimated (Table 5) from its spectrum (Figure 6). The axially symmetric *g* tensor

TABLE 7 Significant charges, bond lengths, dipole moments (*D*), oscillator strengths (*f*) and excitation energies (*E*)

Compound	N(18)	O(26)	M	C(24)=O(26)	N(19)=N(18)	<i>D</i> (D)	<i>f</i>	<i>E</i> (nm)
H <sub>2</sub> L	-0.370013	-0.209119	—	1.363869	1.263122	5.7941	0.0019	503.36
Fe(III)–HL	-0.313167	-0.617981	0.551849	—	—	6.5640	0.0002	8044.21
Cr(III)–HL	-0.347690	-0.656333	0.826656	—	—	5.8226	0.0000	2725.64
Cd(II)–HL	0.243615	0.252231	-0.040645	1.368357	1.263575	5.6894	0.0020	3442.12
Mn(II)–HL	-0.348911	-0.555945	0.372640	—	—	1.7069	0.0005	2487.27
Ni(II)–HL	-0.317903	-0.536607	0.239724	—	—	2.5207	0.0001	8338.81
Cu(ii)–HL	-0.314589	-0.586842	0.492258	1.369257	1.263504	2.1669	0.0011	3868.66
Zn(II)–HL	0.139718	0.202435	0.051785	—	—	3.8270	0.002	2407.69
Co(II)–HL	-0.087261	-0.164942	1.768644	1.369257	1.263448	2.5142	0.0041	2316.63

TABLE 8 QSAR data for sulfa drug ligand (H<sub>2</sub>L)

Function		Function	
Surface area (approx) (Å <sup>2</sup> )	470.12	Total energy (kcal mol <sup>-1</sup> )	-123034.8147206
Surface area (grid) (Å <sup>2</sup> )	632.91	Total energy (a.u.)	-196.068433399
Volume (Å <sup>3</sup> )	1058.46	Binding energy (kcal mol <sup>-1</sup> )	-4734.1908206
Hydration energy (kcal mol <sup>-1</sup> )	-3.89	Isolated atomic energy (kcal mol <sup>-1</sup> )	-118300.6239000
Log <i>P</i>	-1.52	Electronic energy (kcal mol <sup>-1</sup> )	-866861.4656579
Reactivity (Å <sup>3</sup> )	117.29	Core-core interaction (kcal mol <sup>-1</sup> )	743826.6509373
Polarizability (Å <sup>3</sup> )	37.92	Heat of formation (kcal mol <sup>-1</sup> )	52.5541794
Mass (amu)	413.41	Gradient (kcal mol <sup>-1</sup> Å <sup>-1</sup> )	0.0919706

parameters are  $g_{\parallel} > g_{\perp} > 2.0023$ , which indicate that  $d_{x^2-y^2}$  is the ground orbital.<sup>[54]</sup> The *G* factor is determined from  $G = (g_{\parallel} - 2.0023)/(g_{\perp} - 2.0023) = 4$ . In conformity with Hathaway and Billing,<sup>[55]</sup>  $G > 4$  represents a negligible inter-change interaction between copper(II) centres.  $G < 4$  means a significant metal-metal interaction and coincides directly with magnetic moment value. Here, the highly reduced value (1.74) indicates a strong interference between copper centres.<sup>[56,57]</sup> The  $g_{\parallel}$  (2.1606) value matches with relatively covalent M-O and M-N bonds.<sup>[58]</sup> The reduction tendency of  $A_{\parallel}$  towards the increase of  $g_{\parallel}$  points to tetrahedral distortion ( $f = g_{\parallel}/A_{\parallel}$ ).<sup>[59]</sup> In any case, the calculated value is in the range for square planar configuration. Values of  $\sigma^2$  (covale- nce of in-plane  $\sigma$ -bonding) and  $\beta^2$  (covale- nce of in-plane  $\pi$ -bonding) were determined using:  $\alpha^2 = (A_{\parallel}/0.036) + (g_{\parallel} - 2.0023) + 3/7(g_{\perp} - 2.0023) + 0.04$  and  $\beta^2 = (g_{\parallel} - 2.0023)E/ -8\lambda\alpha^2$ , where  $\lambda$  (spin-orbital coupling) =  $-828 \text{ cm}^{-1}$  for free copper ion and  $E$  ( $20\,325 \text{ cm}^{-1}$ ) is the electronic transition energy. The  $\beta^2$  value indicates that the in-plane  $\pi$ -bonding is highly ionic, while the  $\alpha^2$  value indicates that the in-plane  $\sigma$ -bonding is relatively covalent. Dipolar term as a displacement vector between charges inside the complex can be deduced from:  $p = 2\gamma_{Cu}\beta_0\beta_N(r^{-3})$ , where  $\gamma_{Cu}$  is the magnetic moment of copper,  $\beta_0$  is the Bohr magneton,  $\beta_N$  is the nuclear magneton and  $r$  is the distance from nucleus to outer electron shells. The  $p$  value ( $25.55 \times 10^{-4}$ ) does not deviate a lot from known values. The orbital reduction factors,  $K_{\parallel}$  and  $K_{\perp}$ , were also calculated using the following equations:  ${}^2K_{\parallel} = (g_{\parallel} - 2.00277)E/8\lambda$  and  ${}^2K_{\perp} = (g_{\perp} - 2.00277)E/2\lambda$ , where,  ${}^2K_{\parallel} = \alpha^2\beta^2$ . For pure  $\sigma$ - bonding  $K_{\parallel} \approx K_{\perp} \approx -0.77$ , while  ${}^2K_{\parallel} (-0.484) < {}^2K_{\perp} (-1.114)$  signifies in-plane  $\pi$ -bonding, with  ${}^2K_{\perp} < {}^2K_{\parallel}$  accounting for out-of-plane  $\pi$ -bonding.<sup>[60]</sup>

TABLE 9 Docking energies for H<sub>2</sub>L-protein receptor complexes

Receptor	Est. free energy of binding (kcal mol <sup>-1</sup> )	Est. inhibition constant, <i>K<sub>i</sub></i> (μM)	vdW + bond + desolve energy (kcal mol <sup>-1</sup> )	Electrostatic energy (kcal mol <sup>-1</sup> )	Total intercooled energy (kcal mol <sup>-1</sup> )	Frequency (%)	Interact surface
5bmm	-5.60	78.15	-7.52	-0.26	-7.79	20	915.479
5htg	+202.29	-	+199.27	+0.24	+199.51	10	730.722
5j9b	+553.39	-	+547.12	+0.18	+547.30	10	683.538
5ey0	-7.14	5.81	-6.59	-2.04	-8.64	50	812.208
2b0o	-4.38	611.96	-6.61	-0.70	-7.31	30	879.134

### 3.6.1 | Molecular orbital coefficients and bonding parameter calculations

The deduced *g* values are completely different from the elec- tronic value (2.0023). This is attributed to spin-orbit interac- tion with ground state level. Isotropic and anisotropic *g* and *A* parameters were calculated from  $A_0 = (A_{\parallel} + 2A_{\perp})/3$  and  $g_0 = (g_{\parallel} + 2g_{\perp})/3$ . Taking  $A_{\parallel}$  and  $A_{\perp}$  as negative values, the *K* expression is  $K = -(A_0/p) - (g_c - g_0)$ . Thus *K* (Fermi contact term) can be evaluated. The Fermi contact term is an indication of polarization exerted by the uneven apportion- ment of d-electron density on the inner core s-electrons.

### 3.7 | Molecular Modelling, DFT and QSAR Methods

The Gaussian09 program is a theoretical tool implemented to optimize the molecular modelling of the investigated com- pounds. Significant parameters were abstracted from the out- put files based on the numbering schemes.<sup>[61]</sup> Moreover, using the  $E_{\text{HOMO}}$  and  $E_{\text{LUMO}}$  energy gap, essential biological parameters are abstracted.<sup>[61]</sup> Figure 7 shows molecular orbital images for the free drug HOMO and LUMO levels. HOMO level is centred mainly at the methylpyrimidin-2- ylbenzenesulfonamide part enriched with heavy donor atoms although the LUMO levels are spread over the other side donor atoms. This may suggest that the lower energy levels of such atoms participate in a widespread resonance. This may give such atoms a great opportunity for dual nature in charge transfer process of metal to ligand or vice versa. Images of HOMO and LUMO levels for all complexes are displayed in Figure 8(A) and (B), respectively. HOMO images display the approximately unchangeable level posi- tion for all complexes in comparison with free ligand, except Fe(III) and Cr(III) complexes, in which the HOMO level is



TABLE 10 Antibacterial and antifungal activities of H<sub>2</sub>L and metal its complexes<sup>a</sup>

Sample	Inhibition zone diameter (mm per mg sample)			
	<i>E. coli</i> (G <sup>-</sup> )	<i>S. aureus</i> (G <sup>+</sup> )	<i>C. albicans</i> (fungus)	<i>A. fumigatus</i> (fungus)
Control: DMSO	0.0	0.0	0.0	0.0
Standard				
Ampicillin antibacterial agent	22.0	18.0	—	—
Amphotericin B antifungal agent	—	—	19.0	17.0
H <sub>2</sub> L	16.9 ± 0.58	18.2 ± 0.44	13.8 ± 0.25	15.7 ± 0.33
Fe(III) complex (1)	19.6 ± 0.33	22.4 ± 0.58	16.3 ± 0.25	20.2 ± 0.55
Cr(III) complex (2)	9.7 ± 0.3	NA	NA	NA
Cd(II) complex (3)	14.7 ± 0.4	15.1 ± 0.4	10.8 ± 0.4	12.7 ± 0.5
Mn(II) complex (4)	15.9 ± 0.44	19.6 ± 0.19	13.4 ± 0.58	16.8 ± 0.39
Ni(II) complex (5)	17.6 ± 0.58	22.4 ± 0.36	16.7 ± 0.33	20.6 ± 0.58
Cu(II) complex (6)	10.8 ± 0.44	11.7 ± 0.28	11.9 ± 0.25	16.9 ± 0.58
Zn(II) complex (7)	22.3 ± 0.25	14.6 ± 0.42	9.9 ± 0.37	NA
Co(II) complex (8)	16.5 ± 0.25	15.9 ± 0.53	10.2 ± 0.41	NA

<sup>a</sup>Tests done using the diffusion agar technique. Each experiment was conducted at least three times. NA means no activity. The data are expressed in the form of mean ± standard deviation.

relative ionic character for their bonds and coinciding with spectral parameter ( $\beta$ ). The low values for Zn(II), Ni(II), Co(II), Cu(II) and Mn(II) complexes indicate a relatively small distance between charges or lower polarity over all the compound.

### 3.7.2 | Bond lengths, atomic charges and oscillator strengths

Consistent with numbering scheme and using output files, essential bond lengths and charge density over concerned sites were extracted and are summarized in Table 7. Bond lengths concerning coordinating atoms undergo an observable elongation compared to the original free drug. This elongation is directly related to coordination of such atoms. Moreover, charge over N(18) atom is generally reduced which is consistent with its coordination. The charge over O(26) atom is varied, the charge over the atom increasing for five of the complexes and reducing for the other three, Cd(II), Zn(II) and Co(II). The increased values may be due to the replacement of hydrogen with metal atom which increases the bond polarity. While, the reduced values may suggest a strong ligand-to-metal CT. Oscillator strength is an indicator for possible absorption or emission of radiation by the molecule consumed in electronic transitions. Its value is between 0 and 1; a strong transition will have a value close

to 1. The calculated values indicate lower electronic transition efficiency for such electronically condensed metal atoms.

### 3.7.3 | QSAR calculations

Log *P* value is one of the essential results abstracted through QSAR study of the optimized structure using HyperChem software. The structure was approximately optimized by molecular mechanics force field (MM<sup>+</sup>) and followed by full modulation with semi-empirical AM1. The structure was adjusted without confirming any indexes, leading to equilibrium state data. An interconnection between anticancer activity of a drug and its partition coefficient (log *P*) is by an inverse relation.<sup>[65]</sup> Log *P* is the measure of lipophilicity for unionized particles, for which high a log *P* value means little absorption or penetration of drug. For compounds to have a plausible probability of absorption, their values must not be maximal. Here, the calculated value is very low (log *P* = -1.52) which suggests distinct biological behaviour. Also other essential parameters were calculated for optimized structure (Table 8) by applying energy minimization protocol using Polake–Ribiere conjugated gradient algorithm.

### 3.7.4 | Docking analysis

Drug design has benefitted recently from various computational tools using highly sophisticated methods to enhance the designing field. Autodock tools were implemented to clarify the biological features for the new drug to complement the experimental results. This study is interested in designing a new drug that may serve in the biological field, such as antibacterial, antifungal and antitumour activities. The docking process was accomplished using protein receptors of the microorganisms used in the experimental application: 5bmm, 5htg, 5j9b, 5ey0 and 2b0o as hosts for *Escherichia coli*, *Candida albicans*, *Aspergillus fumigatus*, *Staphylococcus aureus* and liver carcinoma cell line,

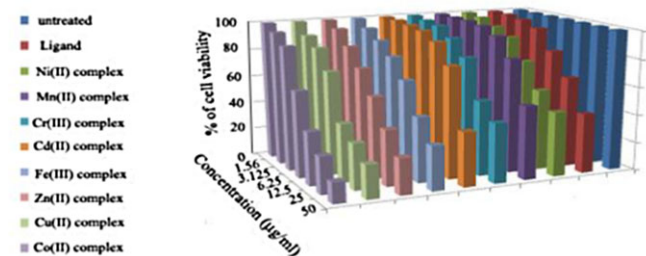


FIGURE 11 *In vitro* cytotoxicity of organic ligand and complexes 1–8 towards human liver carcinoma cell line (HEPG2), compared with standard doxorubicin (Dox) with IC<sub>50</sub> value of 4.73 µg ml<sup>-1</sup>

respectively. The computed energies for the complexes were abstracted and tabulated (Table 9). The binding free energy, constant of inhibition, electrostatic energy, total intercooled energy and receptor–inhibitor complex interact surface are the determined energies. The minimization in binding energy due to mutation may increase the interaction ability toward host receptors.<sup>[66]</sup> The data display significant inhibition activity for 5bmm, 5ey0 and 2b0o receptors, with an absence of this for 5htg and 5j9b. This is based on the instability of the two complexes through their significantly high energies calculated with two protein receptors (5htg and 5j9b) as well as the inhibition constant being completely absent. The docked complexes are presented in Figures 9 and 5S. In agreement with computation, HB plot curves (Figures 10 and 6S) clarify the different modes of interaction, in which the red spots relating to hydrogen-bonding interaction are strongly condensed for 5bmm, 5ey0 and 2b0o receptors and dispersed for 5htg and 5j9b. So, an excellent interaction with 5bmm, 5ey0 and 2b0o protein receptors is expected. Two-dimensional plot curves (7S) verify the mode of interaction inside the docking complexes. The gallery complexes with protein receptors were abstracted and are displayed in 8S. Finally the data suggest superior interaction of the sulfa drug derivative with *E. coli*, *S. aureus* and liver carcinoma in comparison with *C. albicans* and *A. fumigatus*, sufficiently agreeing with experimental results discussed below.

### 3.8 | Biological Investigation

#### 3.8.1 | *In vitro* antibacterial and antifungal activities

*In vitro* antimicrobial activities of H<sub>2</sub>L and metal chelates against *E. coli* (Gram-negative bacteria), *S. aureus* (Gram-positive bacteria), *C. albicans* and *A. fumigatus* were screened using the agar well diffusion method.<sup>[24]</sup> The standard drugs ampicillin and amphotericin B were tested for their antibacterial and antifungal activities at the same concentration and conditions as for the investigated compounds. The results obtained are presented in Table 10. The nanometric nature of the scrutinized chemical compounds is predicted to increase their efficiency in the biological field due to their high surface to volume ratio. They are expected to be highly active due to their ability interact easily with other particles which increase their antimicrobial efficacy.<sup>[67]</sup> The mode of action of the drug and its metal chelates may encompass hydrogen bond formation through N=N and/or OH groups of the ligand or the metal complex and the active position of the cell which disturbs the ordinary cell processes. Also, the compounds may cause turmoil in the respiration system of the organism cells and block the synthesis of proteins which limits the future growth of the tested organisms.<sup>[68]</sup> According to the screening results, in most cases, the investigated compounds show acceptable antimicrobial and antifungal activities towards tested pathogenic bacteria and fungi. H<sub>2</sub>L and Fe(III), Mn(II) and Ni(II) complexes exhibit greater antibacterial activity than the standard

bactericide in use (ampicillin) against *S. aureus*. Zn(III) complex displays higher antibacterial activity than the standard ampicillin towards *E. coli* and Fe(III) complex exhibits strong effectiveness against this bacterium. Fe(III) and Ni(II) complexes present potent activity towards *C. albicans*. Also, Fe(III) and Ni(II) complexes show greater efficacy than the standard drug amphotericin B against *A. fumigatus*. The increased antimicrobial activity upon chelate formation can be attributed to the presence of metal ions which are more hypersensitive towards the microbial cells compared with the organic chelating agent.<sup>[68]</sup> Furthermore, the strengthened influence of the metal chelates may be attributed to the growing lipophilic nature of these compounds upon complexation.<sup>[69]</sup> The coordinating metal ions may block the enzymatic efficiency of cells and/or they may catalyse toxic reactions among cellular constituents. The differences in the activity of distinct complexes across various organisms is a result of either the impermeability of the cells of the microbes or differences in ribosomes in microbial cells.<sup>[70]</sup> The screened organisms are classified as follows: *E. coli* was selected as a representative of Gram-negative bacteria and *S. aureus* as Gram-positive bacteria, *C. albicans* represents unicellular fungi and *A. fumigatus* is a higher fungus which exemplifies multicellular fungi. Consequently, they represent a broad spectrum of test organisms. Hence, the resulting data indicate the potential of the tested azodye ligand and its complexes as novel and highly promising broad-spectrum bactericides and fungicides.

#### 3.8.2 | Antitumour evaluation

Chemotherapy is considered as the major approach for treatment of both metastasized and localized cancer. Also, novel synthetic anticancer curing agents are in great demand to improve the outcome for the great number of patients who relapse after treatment with the presently available cancer therapies.<sup>[71]</sup> Therefore, the synthesized ligand and metal complexes were screened for their *in vitro* cytotoxicity and growth inhibitory activities against human liver carcinoma cell line (HEPG2). The cytotoxicity of the examined samples was measured by median growth inhibitory concentration (IC<sub>50</sub>) required for producing 50% cytotoxic effect towards cancer cells during the tested sample incubation.<sup>[72]</sup> IC<sub>50</sub> is the concentration of tested compound that reduces cell growth by 50% under the naturalistic experimental conditions. Each point was determined from the average of three experiments and specified as the value ± standard deviation. The cytotoxicities of doxorubicin (Dox) drug, H<sub>3</sub>L and metal complexes towards HEPG2 cell line, using different concentrations of Dox and investigated materials, are presented in Figure 11. It is clear from the resulting data that the order of cytotoxic activity (IC<sub>50</sub> values) against HEPG2 cell line of the examined compounds is Co(II) complex, Cu(II) complex, Cr(III) complex, Zn(II) complex, Ni(II) complex, H<sub>2</sub>L, Cd(II) complex, Mn(II) complex and Fe(III) complex in

descending order. These results indicate that the type of metal ion plays an important role in determining the anticancer activity of the tested chemical compounds.<sup>[73]</sup> According to Shier,<sup>[74]</sup> compounds displaying IC<sub>50</sub> less than 5.00 µg ml<sup>-1</sup> are strong anticancer agents, compounds with IC<sub>50</sub> more than 5 and less than 10 µg ml<sup>-1</sup> are considered moderate anticancer agents, while those with IC<sub>50</sub> within the range 10–25 µg ml<sup>-1</sup> are weak anticancer drugs. Accordingly, Co(II) and Cu(II) complexes can be considered moderate anticancer agents whereas the other materials investigated are very weak anticancer agents.

## 4 | CONCLUSIONS

A series of metal ion complexes were prepared using a new sulfa drug derivative. The structural and molecular formulae were investigated spectrally and theoretically. Mono-negative bidentate is the proposed mode of ligand binding towards all metal ions. Octahedral structure is the main feature proposed for most of the complexes. ESR was used to verify the structural formula of Cu(II) complex. XRD patterns and TEM images indicated the nanometre sizes of the investigated compounds. Computational implementation confirmed the proposed geometries through use of the Gaussian09 program. QSAR and docking studies gave a good insight into the expected biological feature of the organic compound. The biological results are the major goal achieved in this study. The data indicate highly promising bactericidal and fungicidal compounds. Also, the antitumour activity results against HEPG2 cell line are acceptable.

## REFERENCES

- [1] R. Arabahmadi, *J. Therm. Anal. Calorim.* **2016**, *123*, 595.
- [2] K. K. Mehta, A. D. Patel, *Acta Chim. Pharm. Indica* **2016**, *6*, 26.
- [3] A. M. Khedr, F. A. Saad, *Turk. J. Chem.* **2015**, *39*, 267.
- [4] N. Van, R. Alabada, O. V. Volyanskii, O. V. Koval'chukova, D. N. Kuznetsov, E. B. Karavaeva, *Fibre Chem.* **2016**, *47*, 497.
- [5] D. Gindre, A. Boeglin, G. Taupier, O. Crégut, J.-P. Vola, A. Barsella, L. Mager, A. Fort, K. D. Dorkenoo, *J. Opt. Soc. Am. B* **2007**, *24*, 532.
- [6] R. Mariselvam, A. J. A. Ranjitsingh, P. M. Selvakumar, A. A. Alarfaj, M. A. Munusamy, *Bioinorg. Chem. Appl.* **2016**, *1*.
- [7] H. E. Gaffar, M. M. G. Fouda, M. E. Khalifa, *Molecules* **2016**, *21*, 122.
- [8] A. M. Khedr, *Chem. Pap.* **2008**, *62*, 541.
- [9] W. H. Ojala, E. A. Sudbeck, L. K. Lu, T. I. Richardson, R. E. Lovrien, W. B. Gleason, *J. Am. Chem. Soc.* **1996**, *118*, 2131.
- [10] D. S. dos Santos, A. Bassi, J. J. Rodrigues, L. Misoguti, O. N. Oliveira, C. R. Mendonça, *Biomacromolecules* **2003**, *4*, 1502.
- [11] B. Blass, *Med. Chem. Lett.* **2016**, *7*, 12.
- [12] S. S. A. Shah, G. Rivera, M. Ashfaq, *Mini-Rev. Med. Chem.* **2016**, *13*, 70.
- [13] H. El-Ghamry, K. Sakai, S. Masaoka, K. El-Baradie, R. Issa, *J. Coord. Chem.* **2012**, *65*, 780.
- [14] A. Z. El-Sonbati, M. A. Diab, M. M. El-Halawany, N. E. Salam, *Spectrochim. Acta A* **2010**, *75*, 755.
- [15] E. H. El-Mossalamy, *Portugaliae Electrochim. Acta* **2009**, *27*, 143.
- [16] A. L. El-Ansary, H. M. Abd El-Fattah, N. S. Abdel-Kader, A. M. Farghaly, *Commun. Inorg. Synth.* **2013**, *1*, 16.
- [17] M. M. Al-Rufaie, *Mod. Chem. Appl.* **2016**, *4*, 1.
- [18] V. A. Modhavadiya, *Orient. J. Chem.* **2012**, *28*, 921.
- [19] R. O. Roblin, J. H. Williams, P. S. Winnek, J. P. English, *J. Am. Chem. Soc.* **1940**, *62*, 2002.
- [20] G. A. A. Al-Hazmia, A. A. El-Zahhar, K. S. Abou-Melha, F. A. Saad, M. H. Abdel-Rhman, A. M. Khedr, N. M. El-Metwaly, *J. Coord. Chem.* **2015**, *68*, 993.
- [21] R. K. Shah, K. S. Abou-Melha, F. A. Saad, T. Yousef, G. A. A. Al-Hazmi, M. G. Elghalban, A. M. Khedr, N. El-Metwaly, *J. Therm. Anal. Calorim.* **2016**, *131*, 731.
- [22] A. M. Khedr, D. F. Draz, *J. Coord. Chem.* **2010**, *63*, 1418.
- [23] A. T. Mubarak, A. Z. El-Sonbati, S. M. Ahmed, *J. Coord. Chem.* **2007**, *60*, 1877.
- [24] A. C. Scott, in *Practical Medical Microbiology*, (Eds: J. G. Collee, J. P. Duguid, A. G. Fraser, B. P. Marmion), Churchill Livingstone, Edinburgh **1981**.
- [25] A. P. Wilson, *Cytotoxicity and Viability Assays in Animal Cell Culture: A Practical Approach*, Oxford University Press, Oxford **2000**.
- [26] T. Mosmann, *J. Immunol. Methods* **1983**, *65*, 55.
- [27] M. J. Frisch et al., *Gaussian 09, Revision D*, Gaussian Inc., Wallingford, CT **2010**.
- [28] R. Dennington, T. Keith, J. Millam, GaussView, Version 4.1.2, Semichem Inc., Shawnee Mission, KS, **2007**.
- [29] T. A. Halgren, *J. Comput. Chem.* **1996**, *17*, 490.
- [30] G. M. Morris, D. S. Goodsell, R. S. Halliday, R. Huey, W. E. Hart, R. K. Belew, A. J. Olson, *J. Comput. Chem.* **1998**, *19*, 1639.
- [31] F. J. Solis, R. J. B. Wets, *Math. Operat. Res.* **1981**, *6*, 19.
- [32] W. J. Geary, *Coord. Chem. Rev.* **1971**, *7*, 81.
- [33] R. M. Issa, K. Y. El-Baradie, N. A. El-Wakiel, *Spectrochim. Acta A* **2004**, *60*, 2883.
- [34] M. S. Refat, I. M. El-Deen, Z. M. Anwer, S. El-Ghol, *J. Mol. Struct.* **2009**, *920*, 149.
- [35] S. I. Al-Saeedi, A. M. A. Alaghaz, R. A. Ammar, *J. Mol. Struct.* **2016**, *1111*, 1.
- [36] F. A. Saad, *Spectrochim. Acta A* **2014**, *128*, 386.
- [37] E. R. Price, J. R. Wasson, *J. Inorg. Nucl. Chem.* **1974**, *36*, 67.
- [38] C. K. Jorgensen, *Prog. Inorg. Chem.* **1962**, *4*, 73.
- [39] S. El-Megharbel, N. El-Metwaly, M. Refat, *Spectrochim. Acta A* **2015**, *149*, 263.
- [40] A. Y. Al-Dawood, N. M. El-Metwaly, H. A. El-Ghamry, *J. Mol. Liq.* **2016**, *220*, 311.
- [41] R. T. Sanderson, *Inorganic Chemistry*, Reinhold, New York **1967**.
- [42] G. Q. Zhong, J. Shen, Q. Y. Jiang, Y. Q. Jia, M. J. Chen, Z. P. Zhang, *J. Therm. Anal. Calorim.* **2008**, *92*, 607.
- [43] J. R. Allan, W. C. Geddes, C. S. Hindle, A. E. Orr, *Thermochim. Acta C* **1989**, *153*, 249.
- [44] F. A. Saad, K. S. Abou-Melha, N. M. El-Metwaly, *Asian J. Chem.* **2015**, *27*, 2678.
- [45] A. W. Coats, J. P. Redfern, *Nature* **1964**, *201*, 68.
- [46] A. A. Frost, R. G. Pearson, *Kinetics and Mechanisms*, Wiley, New York **1961**.
- [47] K. G. Mallikarjun, R. S. Naidu, *Thermochim. Acta* **1992**, *206*, 273.
- [48] U. El-Ayaan, N. M. El-Metwally, M. M. Youssef, S. A. A. El Bialy, *Spectrochimica Acta A* **2007**, *68*, 1278.
- [49] T. M. Ismail, A. M. Khedr, S. M. Abu-El-Wafa, R. M. Issa, *J. Coord. Chem.* **2004**, *57*, 1179.
- [50] A. M. Khedr, S. Jadon, V. Kumar, *J. Coord. Chem.* **2011**, *64*, 1351.
- [51] B. K. Singh, P. Mishra, B. S. Garg, *Transition Met. Chem.* **2007**, *32*, 603.
- [52] J. S. Ritch, T. Chivers, K. Ahmad, M. Afzaal, P. O. Brien, *Inorg. Chem.* **2010**, *49*, 1198.

- [53] N. M. El-Metwaly, M. G. El-Ghalban, *J. Mol. Liq.* **2016**, *220*, 265.
- [54] H. I. Park, L. J. Ming, *J. Inorg. Biochem.* **1998**, *78*, 57.
- [55] B. J. Hathaway, D. E. Billing, *Coord. Chem. Rev.* **1970**, *5*, 143.
- [56] H. Montgomery, E. C. Lingefetter, *Acta Crystallogr.* **1966**, *20*, 728.
- [57] D. Kivelson, R. Neiman, *J. Chem. Phys.* **1961**, *35*, 149.
- [58] R. C. Maurya, S. Rajput, *J. Mol. Struct.* **2004**, *687*, 35.
- [59] J. A. Wellman, F. B. Hulsbergen, *J. Inorg. Nucl. Chem.* **1978**, *40*, 143.
- [60] H. Yokoi, A. W. Addison, *Inorg. Chem.* **1977**, *16*, 1341.
- [61] R. K. Ray, G. R. Kauffman, *Inorg. Chem. Acta* **1990**, *173*, 207.
- [62] I. Fleming, *Frontier Orbitals and Organic Chemical Reactions*, Wiley, London **1976**.
- [63] R. C. Chikate, S. B. Padhye, *Polyhedron* **2005**, *24*, 1689.
- [64] S. Sagdinc, B. Köksoy, F. Kandemirli, S. H. Bayari, *J. Mol. Struct.* **2009**, *917*, 63.
- [65] R. F. George, *Eur. J. Med. Chem.* **2012**, *47*, 377.
- [66] K. Tripathi, R. Muttineni, S. K. Singh, *J. Theor. Biol.* **2013**, *334*, 87.
- [67] S. Amer, N. El-Wakiel, H. El-Ghamry, *J. Mol. Struct.* **2013**, *1049*, 326.
- [68] M. A. Phaniband, S. D. Dhumwad, *Transition Met. Chem.* **2007**, *32*, 1117.
- [69] L. D. S. Yadav, S. Singh, *Indian J. Chem.* **2001**, *40B*, 440.
- [70] B. K. Singh, U. K. Jetley, R. K. Sharma, B. S. Garg, *Spectrochim. Acta A* **2007**, *68*, 63.
- [71] A. S. Sultan, H. Brim, Z. A. Sherif, *Cancer Sci.* **2008**, *2*, 272.
- [72] S. H. Etaiw, S. A. Amer, M. M. El-Bendary, *J. Inorg. Organometal. Polym.* **2011**, *21*, 110.
- [73] X. Riera, V. Moreno, C. J. Ciudad, V. Noe, M. Font-Bardía, X. Solans, *Bioinorg. Chem. Appl.* **2007**, 98732.
- [74] W. T. Shier, *Mammalian Cell Culture on \$5 a Day: A Lab Manual of Low Cost Methods*, University of the Philippines, Los Banos **1991**.

#### SUPPORTING INFORMATION

Additional Supporting Information may be found online in the supporting information tab for this article.

**How to cite this article:** Saad FA, Elghalban MG, El-Metwaly NM, El-Ghamry H, Khedr AM. Density functional theory/B3LYP study of nanometric 4-(2,4-dihydroxy-5-formylphen-1-ylazo)-N-(4-methylpyrimidin-2-yl) benzenesulfonamide complexes: Quantitative structure–activity relationship, docking, spectral and biological investigations. *Appl Organometal Chem.* 2017; e3721. <https://doi.org/10.1002/aoc.3721>